ACS APPLIED MATERIALS & INTERFACES

www.acsami.org Research Article

Sulfur-Embedded FeS_2 as a High-Performance Cathode for Room Temperature All-Solid-State Lithium−Sulfur Batteries

Jean Pierre Mwizerwa,[‖] Qiang Zhang,[‖] Fudong Han, Hongli Wan, Liangting Cai, Chunsheng Wang,* and Xiayin Yao*

Cite This: https://dx.doi.org/10.1021/acsami.0c01607 Read Online

ABSTRACT: All-solid-state lithium−sulfur batteries employing sulfur electrodes and a solid electrolyte at room temperature are still a great challenge owing to the low conductivities of sulfur cathodes. In this work, we report room temperature all-solid-state lithium−sulfur batteries using thin sulfur layer-embedded FeS_2 (FeS_2@S) microsphere composites as active materials in the FeS_2@S−$Li_{10}GeP_2S_{12}$-Super P cathode electrode. Setting the cut-off voltage between 1.5 and 2.8 V, only lithiation−delithiation reactions between L_2FeS_2 and FeS_y and direct reaction between Li_2S and S will occur, which avoids large volume change of FeS_2 caused by the conversion reaction, leading to the structure integrity of FeS_2@S. The resultant batteries exhibit excellent rate and cyclic performances, delivering specific capacities of 1120.9, 937.2, 639.7, 517.2, 361.5, and 307.0 mA h g^{-1} for the FeS_2@S composite cathode, corresponding to the normalized capacities of 1645.5, 1252.9, 782.5, 700.2, 478.4, and 363.6 mA h g^{-1} for sulfur at 30, 50, 100, 500, 1000, and 5000 mA g^{-1}, respectively. Besides, they can retain the normalized capacity of 430.7 mA h g^{-1} for sulfur at 1000 mA g^{-1} after 200 cycles at room temperature.

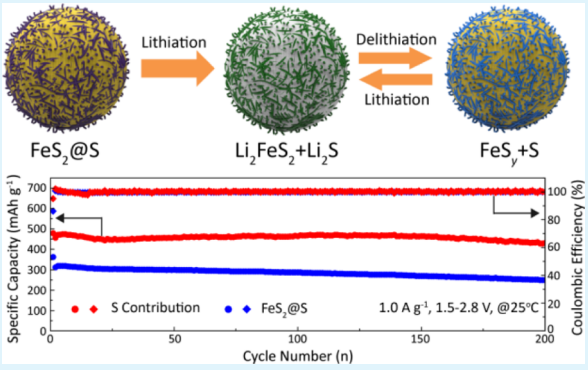

KEYWORDS: *all-solid-state lithium−sulfur battery, stable interface, electronic/ionic conduction, sulfur-embedded FeS_2, electrochemical performance*

1. INTRODUCTION

Lithium−sulfur batteries have attracted substantial attention during the past few years. Sulfur shows intrinsic advantage as a cathode for lithium batteries because of its abundance in nature, nontoxicity, lower cost, high theoretical capacity, and energy density as well as easier ability of manufacturing.[1,2] However, its implementation for large-scale applications, including electric vehicles and stationary uses is still challenging because of (1) dissolution of lithium polysulfide (Li_2S_n) species into organic electrolytes, leading to rapid capacity fading and low Coulombic efficiency, (2) electronic insulating nature of elemental sulfur and lithium sulfide, and (3) huge volume changes of sulfur, causing short cycle life and low reversible capacity of the lithium−sulfur battery.[3] Although great efforts have been devoted to ameliorate the polysulfide shuttling effects,[4,5] the polysulfides are still gradually dissolved in the liquid electrolyte during the cycling process, causing capacity decay, corrosion of the lithium negative electrode, and redox shuttling. Moreover, the safety problem is still an inherent issue in the implementation of liquid electrolyte-based lithium−sulfur batteries.

All-solid-state lithium−sulfur batteries can improve the cyclic performances and safety by eliminating the polysulfide shuttle.[6,7] However, high strain/stress and interface resistance due to the large volume changes during lithiation/delithiation processes cause poor electrochemical performances. Moreover, the insulating nature of the sulfur cathode also reduces the reaction kinetics. Therefore, to enhance electronic/ionic conduction and accommodate the huge volume change of sulfur throughout the lithiation/delithiation process, developing functional sulfur composite materials is needed.

In order to improve the electronic conductivity and further decrease the interfacial resistance, several sulfur composites incorporated with electrically conducting materials, such as carbon nanofibers,[8] reduced graphene oxide,[9] and graphite,[10] were synthesized by gas-phase mixing or mechanical milling. These cells have shown good performances at high temperatures, but economical and eco-friendly batteries have to be operated at lower temperatures ($T \leq 60$ °C).[11,12] It is generally accepted that the lithium-ion transport at the interface is the rate-determining step of the electrochemical reaction.[13,14]

Received: January 27, 2020
Accepted: March 27, 2020
Published: March 27, 2020

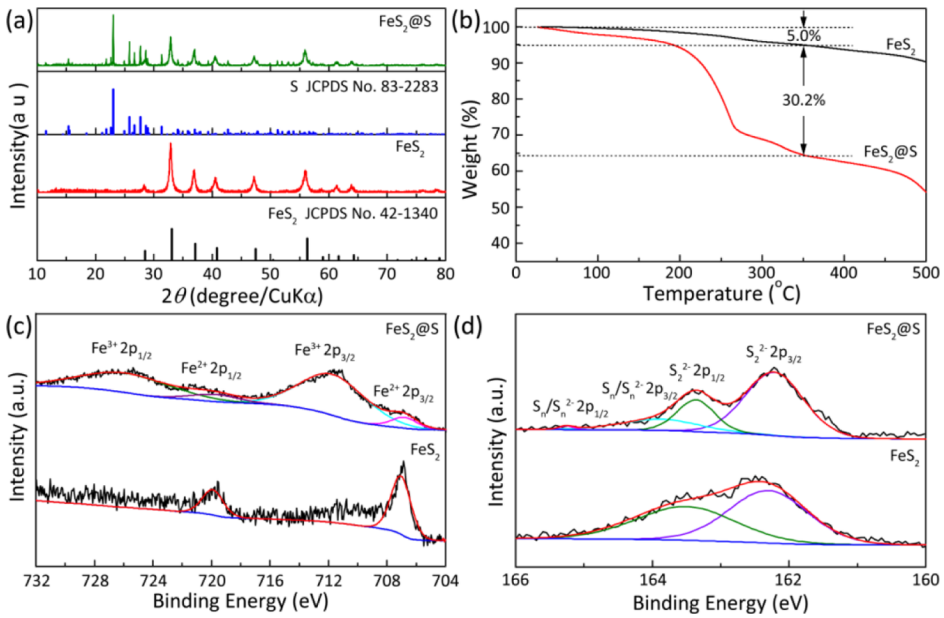

Figure 1. (a) XRD patterns of FeS_2 and FeS_2@S, (b) TGA curves of FeS_2 and FeS_2@S, and high-resolution XPS spectra of the as-synthesized FeS_2 and FeS_2@S in (c) Fe region and (d) S region.

Improving lithium-ion conduction and contact areas could achieve better electrochemical performances. Recently, transition metal disulfides, such as CoS_2,[15] WS_2,[16] and TiS_2,[17] have been investigated as conductive fillers and polysulfide captures in traditional lithium−sulfur batteries owing to their superior interactions between the metal cation and the polysulfide anion, and high specific surface areas. In addition, transition metal sulfides exhibit excellent electrochemical performances because of the better interfacial compatibility and stability with sulfide solid electrolytes.

Iron pyrite (FeS_2) is a typical member of transition metal disulfides with the merits of abundance in nature, environmental benignity, and raw material cost effectiveness. Meanwhile, FeS_2 shows great potential as a cathode for lithium-ion batteries because of its superior electronic/ionic conduction, high theoretical specific capacity, and moderate voltage plateau.[18] FeS_2 can serve as not only a polysulfide species immobilizer in a sulfur composite electrode but also as buffer to relieve the large volume expansion of an active material.[19,20] Hence, iron pyrite as the host for the sulfur cathode is likely to enhance reversible capacity and cyclic performances. There is a report of using FeS_2−sulfur cathodes prepared with the simple ball-milling process for all-solid-state batteries. However, the performance of that cathode is still much limited to 20 cycles mainly because of the insufficient contact between S and FeS_2. Engineering FeS_2−sulfur electrode to ensure a great interfacial contact between FeS_2 and S is therefore important to improve the performance of this cathode.[21]

Herein, pure FeS_2 and FeS_2@S microsphere composite electrode materials were synthesized using a liquid-phase strategy. Furthermore, the electrochemical performances of both FeS_2 and FeS_2@S microsphere cathode materials were investigated in all-solid-state lithium−sulfur batteries at room temperature. Reversible capacities of 632.4 and 922.5 mA h g^{-1} are delivered for FeS_2 and FeS_2@S, respectively after 20 cycles at 30 mA g^{-1}, corresponding to the sulfur contribution of 1592.9 mA h g^{-1}. Even at 1000 mA g^{-1}, it still maintains a normalized discharge capacity of 430.7 mA h g^{-1} for sulfur after 200 cycles. The high reversible capacity and excellent cyclic performances of the FeS_2@S cathode can be ascribed to its superior ionic/electronic conduction, smaller volume change, and elimination of the polysulfide shuttle.

2. RESULTS AND DISCUSSION

X-ray diffraction (XRD) patterns of the as-synthesized FeS_2 and FeS_2@S composite samples are illustrated in Figure 1a. Clearly, the sharp characteristic diffraction peaks of FeS_2 can be indexed to cubic iron pyrite (JCPDS card no. 42-1340). No diffraction peaks resulting from impurities were detected, indicating that highly pure and well-developed FeS_2 is obtained by a facile liquid-phase method. For the FeS_2@S sample, with the exception of distinguishable diffraction peaks from pyrite FeS_2, all other strong diffraction peaks stem from elemental sulfur, which is in accordance with orthorhombic elemental sulfur (JCPDS card no. 83-2283), confirming the presence of sulfur in FeS_2. The S and Fe contents in the FeS_2@S sample were determined using inductively coupled plasma optical emission spectrometry (ICP−OES), and the results show that the FeS_2@S composite contains 70.1 wt % FeS_2 and 29.9 wt % active sulfur. Thermogravimetric analysis (TGA) was conducted to further determine the sulfur content for the FeS_2@S composite, as shown in Figure 1b. The sulfur content was estimated to be 30.2 wt %, which is consistent with ICP−OES results. Clearly, the temperature for sulfur evaporation in FeS_2@S is between 100 and 350 °C.[22,23]

X-ray photoelectron spectroscopy (XPS) was performed to further identify the chemical composition of the as-synthesized FeS_2 and FeS_2@S samples. Figure 1c shows the high-resolution XPS spectrum of Fe 2p for both FeS_2 and FeS_2@S. For FeS_2, the dominating peaks located at 720.3 and 707.1 eV, corresponding to Fe $2p_{1/2}$ and Fe $2p_{3/2}$ of the Fe^{2+} state, respectively.[24,25] The Fe 2p spectra of FeS_2@S also contain the major peaks of Fe $2p_{1/2}$ spectra located at 726.4 eV and Fe $2p_{3/2}$ spectra at 712.4 eV, which are attributed to the Fe^{3+} state.[26] The chemical shift of Fe 2p can be ascribed to the electrostatic interaction between Fe^{2+} and elemental S in the

https://dx.doi.org/10.1021/acsami.0c01607
ACS Appl. Mater. Interfaces XXXX, XXX, XXX−XXX

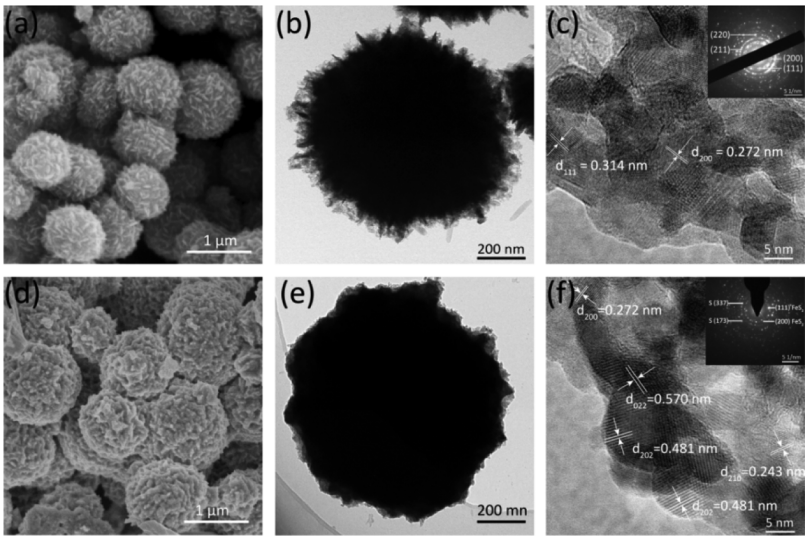

Figure 2. SEM, TEM, and HRTEM images and the corresponding SAED patterns (insets) of the synthesized (a−c) FeS_2 and (d−f) FeS_2@S.

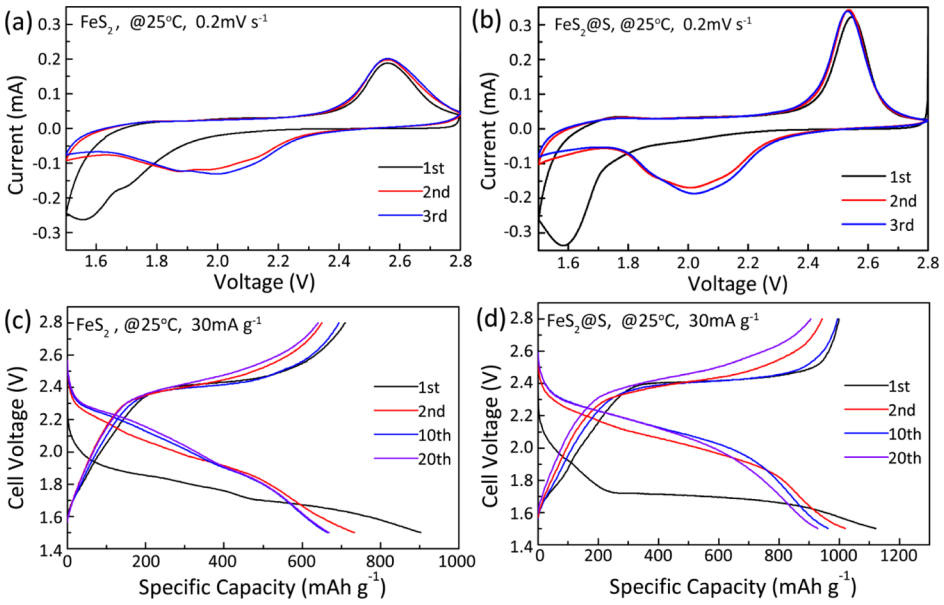

Figure 3. CV of (a) FeS_2 and (b) FeS_2@S electrodes between 1.5 and 2.8 V at a scan rate of 0.2 mV s^{-1} for the first three cycles. Discharge−charge profiles for (c) FeS_2 and (d) FeS_2@S electrodes at 30 mA g^{-1}.

FeS_2@S sample. Figure 1d reveals fitting analysis of S 2p spectra of FeS_2 and FeS_2@S samples, showing spectra corresponding to the various species of sulfur. As can be seen, the peaks located at 163.5 and 162.8 eV are attributed to S $2p_{1/2}$ and S $2p_{1/2}$ of S_2^{2-} ions in both FeS_2 and FeS_2@S samples, respectively, whereas the peaks at 165.1 and 164.0 eV can be assigned to S_n or S_n^{2-} in FeS_2@S samples, which correspond to the presence of elemental S and the interaction between FeS_2 and S in FeS_2@S samples, respectively.[27]

The morphologies of the as-synthesized FeS_2 and FeS_2@S samples were observed by scanning electron microscopy (SEM) and transmission electron microscopy (TEM), as shown in Figure 2. The homogeneous FeS_2 microspheres with a diameter of about 1 μm show a 50 nm-thick shell consisting of numerous outgrown spine-like nanoparticles (Figure 2a,b). After incorporating sulfur in FeS_2, the dense FeS_2@S samples still maintain the microsphere morphology with no obvious size change. However, these nanoparticles at the surface of FeS_2@S samples disappear, illustrating that elemental sulfur has been successfully confined in the shell of FeS_2 microspheres with a thickness of about 50 nm (Figure 2d,e), indicating that FeS_2 may be used as a suitable host for sulfur. High-resolution TEM (HRTEM) and selected area electron diffraction (SAED) were conducted to further reveal the microstructures of as-synthesized FeS_2 and FeS_2@S samples (Figure 2c,f). The HRTEM image of a typical edge-view of FeS_2 microspheres (Figure 2c) illustrates a clear lattice fringe spacing of 0.31 and 0.27 nm, corresponding to the (111) and (200) lattice planes of pyrite FeS_2, respectively, which are consistent with XRD results, indicating a well-developed crystal structure of the obtained FeS_2 microspheres. The corresponding SAED patterns consist of several diffraction rings which can be indexed to (111), (200), (211), and (220) from inside out, further confirming the well-developed structure of FeS_2 microspheres. Compared to FeS_2 microspheres, the HRTEM image of FeS_2@S microspheres shows

https://dx.doi.org/10.1021/acsami.0c01607
ACS Appl. Mater. Interfaces XXXX, XXX, XXX−XXX

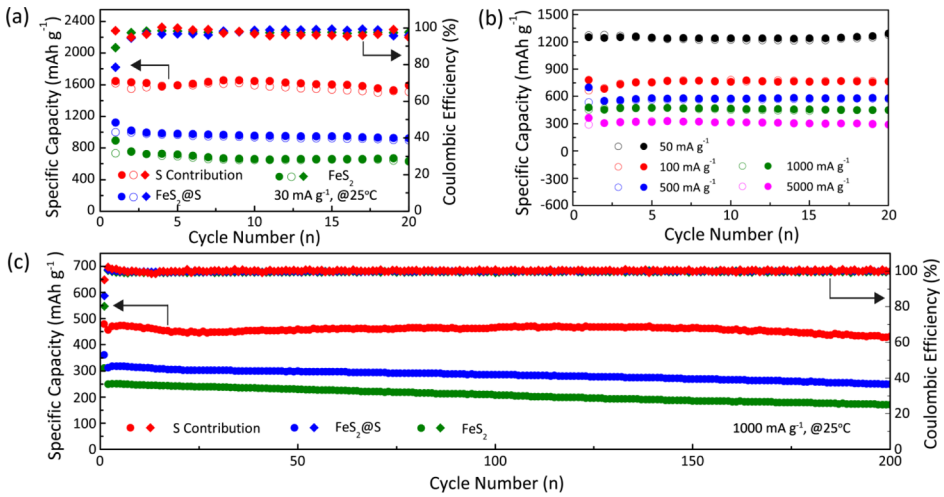

Figure 4. Electrochemical performances of FeS_2 and FeS_2@S electrodes as cathodes in all-solid-state lithium−sulfur cells. (a) Cycling performance of FeS_2 and FeS_2@S and the capacity contribution of S at 30 mA g^{-1} under room temperature. (b) Sulfur contribution at 50, 100, 500, 1000, and 5000 mA g^{-1}. (c) Cyclic performances of the FeS_2@S composite and FeS_2 electrodes and the sulfur contribution in all-solid-state lithium−sulfur batteries at 1000 mA g^{-1} for 200 cycles at room temperature.

both lattice spaces for both sulfur and FeS_2 (Figure 2f). The interplanar spacing of 0.570 and 0.481 nm agrees well with the (022) and (202) lattice planes of sulfur, respectively, while the lattice spacing of 0.272 and 0.243 nm corresponds to the (200) and (210) lattice planes of FeS_2, respectively. The corresponding SAED pattern further proves the coexistence of both sulfur and FeS_2 in FeS_2@S microspheres.

The electrochemical performances of the as-synthesized FeS_2 and FeS_2@S composite electrodes were investigated in both solid and liquid electrolyte-based lithium−sulfur cells at room temperature. The commonly accepted reaction mechanism for FeS_2 within 0.5−3.0 V can be expressed as follows[28−32]

$$FeS_2 + 2Li^+ + 2e^- \rightarrow Li_2FeS_2 \quad (1)$$

$$Li_2FeS_2 + 2Li^+ + 2e^- \rightarrow 2Li_2S + Fe \quad (2)$$

$$2Li_2S + Fe \rightarrow Li_2FeS_2 + 2Li^+ + 2e^- \quad (3)$$

$$Li_2FeS_2 \leftrightarrow Li_{2-x}FeS_2 + xLi^+ + xe^- \qquad (0.5 < x < 0.8) \quad (4)$$

$$Li_{2-x}FeS_2 \leftrightarrow FeS_y + (2-y)S + (2-x)Li^+ + (2-x)e^- \quad (5)$$

The cyclic voltammograms of the as-synthesized materials were recorded at a scan rate of 0.2 mV s^{-1}. Figure S1 displays cyclic voltammetry (CV) curves of FeS_2 within 0.5−3.0 V, showing two reduction peaks at around 1.6 and 1.2 V in the initial cathodic scan, which are associated with reaction 1 $FeS_2 + 2Li^+ + 2e^- \rightarrow Li_2FeS_2$ (1.6 V) and reaction 2 $Li_2FeS_2 + 2Li^+ + 2e^- \rightarrow 2Li_2S + Fe$ (1.2 V), respectively. However, these peaks vanish in the following cycles, indicating different reaction kinetics and pathways between the first and the following ones. In the delithiation cycles, oxidation peaks at 1.9 V is related to the formation of Li_2FeS_2 with reaction 3 $2Li_2S + Fe \rightarrow Li_2FeS_2 + 2Li^+ + 2e^-$, and the peak at 2.5 V is attributed to reaction 4 $Li_2FeS_2 \rightarrow Li_{2-x}FeS_2 + xLi^+ + xe^-$ and reaction 5 $Li_{2-x}FeS_2 \rightarrow FeS_y + (2-y)S + (2-x)Li^+ + (2-x)e^-$. After the first cycle, the appearance of an obvious reduction peak at 2.0 V is caused by the formation of Li_2FeS_2, and a peak at 1.4 V is attributable to reaction 2 $Li_2FeS_2 + 2Li^+ + 2e^- \rightarrow 2Li_2S + Fe$, further confirming an irreversible phase change occurred after the first cycle. When cycled between 1.5 and 2.8 V (Figure 3a), only one reduction peak at around 1.6 V is observed, confirming that reaction 2 is absent and the corresponding oxidation peak related to reaction 3 also vanished. For the FeS_2@S electrode (Figure 3b), the curve for the first cycle is similar to that for the FeS_2 electrode. However, in the following cycles, the reactions related to FeS_y and S both occur. Because the voltage of oxidation−reduction peaks for FeS_y is close to that of S, in the following lithiation−delithiation process, the pair of peaks at 2.0 and 2.5 V is related to the reversible reaction of $FeS_y + (2-y)S + 2Li^+ + 2e^- \leftrightarrow Li_2FeS_2$ and the reduction−oxidation of sulfur.

By comparison, coin cells employing FeS_2@S cathodes were also investigated using a liquid organic electrolyte. Figure S2 shows the CV curves of the FeS_2@S cathode at a cut-off voltage of 1.5−2.8 V. As can be observed for the initial cycle, a reduction peak corresponding to the lithiation of FeS_2 was seen at 1.6 V[33] and two reduction peaks at approximately 2.05 and 2.28 V, respectively, which are ascribed to the transitions of sulfur to a long-chain polysulfide and a long-chain to low-order polysulfide.[34] The CV curve of FeS_2@S displays only one sharp oxidation peak in the first and subsequent cycles at 2.5 V, which is ascribed to the delithiation process of Li_2FeS_2 to FeS_y and sulfur and conversion of Li_2S to Li_2S_n and finally to S.[35]

The galvanostatic discharge−charge profiles of the FeS_2 and FeS_2@S composite in all-solid-state lithium−sulfur cells at 30 mA g^{-1} under room temperature are shown in Figure 3c,d. Only one voltage plateau at 1.7 V is observed in the first discharge curve, while this plateau shifts to 2.1 V in the following cycles (Figure 3c,d), which is consistent to the reduction peak in the CV curves. No discharge plateau of elemental S was detected in FeS_2@S electrodes, which could be ascribed to the electrostatic interaction between Fe^{2+} and elemental S in the FeS_2@S sample. A more obvious charge plateau at 2.4 V and an increased discharge capacity are observed for the FeS_2@S electrode (Figure 3d) compared to that for the FeS_2 electrode (Figure 3c), further confirming that FeS_2 and S will react simultaneously during charge−discharge

https://dx.doi.org/10.1021/acsami.0c01607
ACS Appl. Mater. Interfaces XXXX, XXX, XXX−XXX

processes. Besides, only one discharge plateau at around 2.1 V after the first cycle is present for the FeS_2@S electrode in the all-solid-state lithium−sulfur battery, which is different from that in the liquid electrolyte-based lithium−sulfur battery, where the discharge curves show two discharge plateaus at 2.35 and 2.05 V and two charge plateaus at 2.25 and 2.4 V.[36] Figure S3 shows discharge−charge profiles of the FeS_2@S cathode using liquid electrolytes within cut-off potentials of 1.5−2.8V at 50 mA g^{-1}. The discharge and charge profiles are related to FeS_2 and sulfur cathodes, which are consistent with previous studies,[37−39] indicating the viability of the FeS_2@S cathode in the conventional lithium−sulfur cell. This difference strongly supports the hybrid reaction mechanism of Li−FeS_y and Li−S during the discharge−charge process for the FeS_2@S electrode in the all-solid-state lithium−sulfur battery. In addition, the discharge−charge curves of the FeS_2 electrode in a solid cell between 0.5 and 3.0 V show two discharge plateaus at 2.2 and 1.4 V and two charge plateaus at 1.8 and 2.4 V after the first cycle (Figure S4), further confirming two electron storage occurred for FeS_2 when cycling within 1.5−2.8 V.

In order to demonstrate the sulfur reactivity at room temperature, sulfur contribution to the capacity was investigated in an all-solid-state battery. Cyclic performances of FeS_2 and FeS_2@S composite electrodes are compared (Figure 4a). The results reveal that the FeS_2@S composite electrode delivered a high initial discharge capacity of 1120.9 mA h g^{-1}, corresponding to the normalized discharge capacity of 1645.5 mA h g^{-1} for sulfur with an extraordinary high initial Coulombic efficiency of 98.5% under 30 mA g^{-1}. After cycling for 20 cycles, FeS_2 and FeS_2@S composite electrodes maintain discharge capacities of 632.4 and 922.5 mA h g^{-1}, respectively, equivalent to the normalized capacity of 1592.9 mA h g^{-1} for the sulfur. The high rate capability of FeS_2 and FeS_2@S composite electrodes was further investigated at 50, 100, 500, 1000, and 5000 mA g^{-1}. The results show that discharge capacities of 800.6, 577.9, 438.0, 310.9, and 282.5 mA h g^{-1} for FeS_2 (Figure S5) and 937.2, 639.7, 517.2, 361.5, and 307.0 mA h g^{-1} for FeS_2@S (Figure S6) are delivered, corresponding to the normalized capacities of 1252.9, 782.5, 700.2, 478.4, and 363.6 mA h g^{-1} for sulfur (Figure 4b). FeS_2 and FeS_2@S composite electrodes also exhibit excellent cycling stability under different current densities within 20 cycles (Figure S7).

The cyclic performances of the FeS_2@S composite, FeS_2 electrodes, and the sulfur contribution were also investigated (Figure 4c). The normalized capacity of 430.7 mA h g^{-1} for sulfur was obtained at 1000 mA g^{-1} after 200 cycles. Accordingly, the discharge capacity remains at 249.5 and 171.1 mA h g^{-1} for FeS_2@S and FeS_2 electrodes, respectively. By comparison, the FeS_2@S composite electrode in liquid organic electrolytes suffers from rapid capacity decay with low Coulombic efficiency because of polysulfide dissolution and shuttle reaction, which will reduce the active material utilization (Figure S8). The extraordinary electrochemical performance for the FeS_2@S composite electrode might be caused by the following factors: First, eliminating the conversion reaction of FeS_2 by choosing a cut-off voltage of 1.5−2.8 V can decrease volume expansion of FeS_2, which will provide a stable host for sulfur, thus preventing the pulverization of the cathode material. Second, the strong interaction between highly electrical conductive FeS_y and S can maintain the solid−solid interfacial contact even though volume expansion of sulfur occurred during cycling, which will improve the cycling stability. Moreover, a different reaction mechanism for sulfur by using solid electrolytes can prevent the production and shuttle reaction of polysulfide species, which will improve the mass utilization and reversible capacity. The electrochemical performance of the as-prepared FeS_2@S cathode is one of the best among the reported all-solid-state lithium−sulfur batteries based on FeS_2@S and S@C cathodes (Table S1).[9,21,32,40−49]

3. CONCLUSIONS

In summary, FeS_2 and FeS_2@S composites are synthesized with a liquid-phase approach, showing uniform distribution of microsized spheres consisting of tightly aggregated nanoparticles. Both FeS_2 and FeS_2@S microspheres were employed as cathode materials in all-solid-state lithium−sulfur batteries at room temperature. FeS_2@S composites show specific capacities of 1120.9, 937.2, 639.7, 517.2, 361.5, and 307.0 mA h g^{-1} at 30, 50, 100, 500, 1000, and 5000 mA g^{-1}, respectively, corresponding to the normalized capacity of 1645.5, 1252.9, 782.5, 700.2, 478.4, and 363.6 mA h g^{-1} for sulfur in all-solid-state lithium−sulfur cells. The cells maintain the normalized specific capacity of about 430.7 mA h g^{-1} for sulfur after 200 cycles at 1000 mA g^{-1}. The successful demonstration of the high power rate and excellent cycling stability for the FeS_2@S composite in room-temperature all-solid-state lithium−sulfur batteries could be reasonably attributed to the stable FeS_2 host for sulfur, enabling high capacity contribution of sulfur and efficient contact between FeS_2@S and the highly ionic conductive $Li_{10}GeP_2S_{12}$ solid electrolyte, resulting in the formation of a stable interface with smooth fast electron and ion conductions across the composite positive electrode and sulfide solid electrolyte. Clearly, the environmentally benign, low-cost pyrite showed a competitive sulfur host electrode material for all-solid-state lithium−sulfur batteries at room temperature.

■ ASSOCIATED CONTENT

Supporting Information

The Supporting Information is available free of charge at https://pubs.acs.org/doi/10.1021/acsami.0c01607.

Detailed experimental methods; CV curves of FeS_2 as a cathode material of all-solid-sate lithium batteries recorded at a scan rate of 0.2 mV s^{-1} between 0.5 and 3.0 V (vs Li/Li^+) at room temperature; CV profiles of the FeS_2@S electrode with an organic liquid electrolyte between 1.5 and 2.8 V (vs Li/Li^+) at a scan rate of 0.2 mV s^{-1}; discharge−charge voltage profiles for the FeS_2@S electrode at 50 mA g^{-1} with organic liquid electrolyte between 1.5 and 2.8 V; discharge−charge profiles for FeS_2 in all-solid-state lithium batteries between 0.5 and 3.0 V; discharge−charge profiles for FeS_2 and FeS_2@S electrodes in all-solid-state batteries at 50, 100, 500, 1000, and 5000 mA g^{-1} between 1.5 and 2.8 V; cycling performances of FeS_2 and FeS_2@S electrodes in all-solid-state lithium batteries at 50, 100, 500, 1000, and 5000 mA g^{-1} under room temperature; cycling performances of lithium−sulfur cells with the FeS_2@S composite at 50 mA g^{-1} in organic liquid electrolyte under room temperature; and comparison of the electrochemical performance of the FeS_2@S cathode to the reported all-solid-state lithium−sulfur batteries (PDF)

https://dx.doi.org/10.1021/acsami.0c01607
ACS Appl. Mater. Interfaces XXXX, XXX, XXX−XXX

AUTHOR INFORMATION

Corresponding Authors

Chunsheng Wang − *Department of Chemical and Biomolecular Engineering, Department of Chemistry and Biochemistry, University of Maryland, College Park, Maryland 20742, United States;* orcid.org/0000-0002-8626-6381; Email: cswang@umd.edu

Xiayin Yao − *Ningbo Institute of Materials Technology and Engineering, Chinese Academy of Sciences, 315201 Ningbo, P. R. China; Center of Materials Science and Optoelectronics Engineering, University of Chinese Academy of Sciences, Beijing 100049, P. R. China;* orcid.org/0000-0002-2224-4247; Email: yaoxy@nimte.ac.cn

Authors

Jean Pierre Mwizerwa − *Ningbo Institute of Materials Technology and Engineering, Chinese Academy of Sciences, 315201 Ningbo, P. R. China; Center of Materials Science and Optoelectronics Engineering, University of Chinese Academy of Sciences, Beijing 100049, P. R. China*

Qiang Zhang − *Ningbo Institute of Materials Technology and Engineering, Chinese Academy of Sciences, 315201 Ningbo, P. R. China; Center of Materials Science and Optoelectronics Engineering, University of Chinese Academy of Sciences, Beijing 100049, P. R. China*

Fudong Han − *Department of Chemical and Biomolecular Engineering, Department of Chemistry and Biochemistry, University of Maryland, College Park, Maryland 20742, United States*

Hongli Wan − *Ningbo Institute of Materials Technology and Engineering, Chinese Academy of Sciences, 315201 Ningbo, P. R. China; Center of Materials Science and Optoelectronics Engineering, University of Chinese Academy of Sciences, Beijing 100049, P. R. China*

Liangting Cai − *Ningbo Institute of Materials Technology and Engineering, Chinese Academy of Sciences, 315201 Ningbo, P. R. China*

Complete contact information is available at: https://pubs.acs.org/10.1021/acsami.0c01607

Author Contributions

[‖]J.P.M. and Q.Z. contributed equally.

Notes

The authors declare no competing financial interest.

ACKNOWLEDGMENTS

The work was supported by funding from the National Key R&D Program of China (grant no. 2018YFB0905400), the National Natural Science Foundation of China (grant nos. 51872303, U1964205), the Zhejiang Provincial Natural Science Foundation of China (grant nos. LD18E020004, LY18E020018), the Ningbo S&T Innovation 2025 Major Special Programme (grant nos. 2018B10061, 2018B10087, 2019B10044), the Jiangxi Provincial Key R&D Program of China (grant no. 20182ABC28007), and the Youth Innovation Promotion Association CAS (2017342).

REFERENCES

(1) Bruce, P. G.; Freunberger, S. A.; Hardwick, L. J.; Tarascon, J.-M. Li-O_2 and Li-S Batteries with High Energy Storage. *Nat. Mater.* **2011**, *11*, 19−29.

(2) Yang, Y.; Yu, G.; Cha, J. J.; Wu, H.; Vosgueritchian, M.; Yao, Y.; Bao, Z.; Cui, Y. Improving the Performance of Lithium-Sulfur Batteries by Conductive Polymer Coating. *ACS Nano* **2011**, *5*, 9187−9193.

(3) Kolosnitsyn, V. S.; Karaseva, E. V. Lithium-Sulfur Batteries: Problems and Solutions. *Russ. J. Electrochem.* **2008**, *44*, 506−509.

(4) Yuan, H.; Chen, X.; Zhou, G.; Zhang, W.; Luo, J.; Huang, H.; Gan, Y.; Liang, C.; Xia, Y.; Zhang, J.; Wang, J.; Tao, X. Efficient Activation of Li_2S by Transition Metal Phosphides Nanoparticles for Highly Stable Lithium−Sulfur Batteries. *ACS Energy Lett.* **2017**, *2*, 1711−1719.

(5) Chung, S.-H.; Luo, L.; Manthiram, A. TiS_2-Polysulfide Hybrid Cathode with High Sulfur Loading and Low Electrolyte Consumption for Lithium-Sulfur Batteries. *ACS Energy Lett.* **2018**, *3*, 568−573.

(6) Wang, S.; Ding, Y.; Zhou, G.; Yu, G.; Manthiram, A. Durability of the $Li_{1+x}Ti_{2-x}Al_x(PO_4)_3$ Solid Electrolyte in Lithium-Sulfur Batteries. *ACS Energy Lett.* **2016**, *1*, 1080−1085.

(7) Xin, S.; You, Y.; Wang, S.; Gao, H.-C.; Yin, Y.-X.; Guo, Y.-G. Solid-State Lithium Metal Batteries Promoted by Nanotechnology: Progress and Prospects. *ACS Energy Lett.* **2017**, *2*, 1385−1394.

(8) Yamada, T.; Ito, S.; Omoda, R.; Watanabe, T.; Aihara, Y.; Agostini, M.; Ulissi, U.; Hassoun, J.; Scrosati, B. All Solid-state Lithium-Sulfur Battery using a Glass-type P_2S_5-Li_2S Electrolyte: Benefits on Anode Kinetics. *J. Electrochem. Soc.* **2015**, *162*, A646−A651.

(9) Yao, X.; Huang, N.; Han, F.; Zhang, Q.; Wan, H.; Mwizerwa, J. P.; Wang, C.; Xu, X. High-Performance All-Solid-State Lithium-Sulfur Batteries Enabled by Amorphous Sulfur-Coated Reduced Graphene Oxide Cathodes. *Adv. Energy Mater.* **2017**, *7*, 1602923.

(10) Agostini, M.; Aihara, Y.; Yamada, T.; Scrosati, B.; Hassoun, J. A Lithium-Sulfur Battery Using a Solid, Glass-type P_2S_5-Li_2S Electrolyte. *Solid State Ionics* **2013**, *244*, 48−51.

(11) Lin, Z.; Liu, Z.; Fu, W.; Dudney, N. J.; Liang, C. Lithium Polysulfidophosphates: a Family of Lithium-Conducting Sulfur-Rich Compounds for Lithium-Sulfur Batteries. *Angew. Chem., Int. Ed.* **2013**, *52*, 7460−7463.

(12) Hakari, T.; Hayashi, A.; Tatsumisago, M. Highly Utilized Lithium Sulfide Active Material by Enhancing Conductivity in All-Solid-State Batteries. *Chem. Lett.* **2015**, *44*, 1664−1666.

(13) Zhang, Q.; Mwizerwa, J. P.; Wan, H.; Cai, L.; Xu, X.; Yao, X. Fe_3S_4@$Li_7P_3S_{11}$ Nanocomposites as Cathode Materials for All-Solid-State Lithium Batteries with Improved Energy Density and Low Cost. *J. Mater. Chem. A* **2017**, *5*, 23919−23925.

(14) Takada, K. Progress and Prospective of Solid-State Lithium Batteries. *Acta Mater.* **2013**, *61*, 759−770.

(15) Zhou, J.; Lin, N.; Cai, W. l.; Guo, C.; Zhang, K.; Zhou, J.; Zhu, Y.; Qian, Y. Synthesis of S/CoS_2 Nanoparticles-embedded N-doped Carbon Polyhedrons from Polyhedrons ZIF-67 and Their Properties in Lithium-Sulfur Batteries. *Electrochim. Acta* **2016**, *218*, 243−251.

(16) Lei, T.; Chen, W.; Huang, J.; Yan, C.; Sun, H.; Wang, C.; Zhang, W.; Li, Y.; Xiong, J. Multi-Functional Layered WS_2 Nanosheets for Enhancing the Performance of Lithium-Sulfur Batteries. *Adv. Energy Mater.* **2017**, *7*, 1601843.

(17) Sun, K.; Zhang, Q.; Bock, D. C.; Tong, X.; Su, D.; Marschilok, A. C.; Takeuchi, K. J.; Takeuchi, E. S.; Gan, H. Interaction of TiS_2 and Sulfur in Li-S Battery System. *J. Electrochem. Soc.* **2017**, *164*, A1291−A1297.

(18) Cheng, S.; Wang, J.; Lin, H.; Li, W.; Qiu, Y.; Zheng, Z.; Zhao, X.; Zhang, Y. Improved Cycling Stability of the Capping Agent-free Nanocrystalline FeS_2 Cathode *via* an Upper Cut-off Voltage Control. *J. Mater. Sci.* **2016**, *52*, 2442−2451.

(19) Zhang, S. S.; Tran, D. T. Pyrite FeS_2 as an Efficient Adsorbent of Lithium Polysulphide for Improved Lithium-Sulphur Batteries. *J. Mater. Chem. A* **2016**, *4*, 4371−4374.

(20) Sun, K.; Cama, C. A.; DeMayo, R. A.; Bock, D. C.; Tong, X.; Su, D.; Marschilok, A. C.; Takeuchi, K. J.; Takeuchi, E. S.; Gan, H. Interaction of FeS_2 and Sulfur in Li-S Battery System. *J. Electrochem. Soc.* **2016**, *164*, A6039−A6046.

(21) Ulissi, U.; Ito, S.; Hosseini, S. M.; Varzi, A.; Aihara, Y.; Passerini, S. High Capacity All-Solid-State Lithium Batteries Enabled by Pyrite-Sulfur Composites. *Adv. Energy Mater.* **2018**, *8*, 1801462.

(22) Yang, X.; Zhang, L.; Zhang, F.; Huang, Y.; Chen, Y. Sulfur-Infiltrated Graphene-Based Layered Porous Carbon Cathodes for High-Performance Lithium-Sulfur Batteries. *ACS Nano* **2014**, *8*, 5208−5215.
(23) Zhao, Z.; Wang, S.; Liang, R.; Li, Z.; Shi, Z.; Chen, G. Graphene-wrapped Chromium-MOF(MIL-101)/Sulfur Composite for Performance Improvement of High-Rate Rechargeable Li-S Batteries. *J. Mater. Chem. A* **2014**, *2*, 13509−13512.
(24) Wang, D.; Wang, Q.; Wang, T. Shape Controlled Growth of Pyrite FeS_2 Crystallites *via* a Polymer-assisted Hydrothermal Route. *CrystEngComm* **2010**, *12*, 3797−3805.
(25) Descostes, M.; Mercier, F.; Thromat, N.; Beaucaire, C.; Gautier-Soyer, M. Use of XPS in the Determination of Chemical Environment and Oxidation State of Iron and Sulfur Samples: Constitution of a Data Basis in Binding Energies for Fe and S Reference Compounds and Applications to the Evidence of Surface Species of an Oxidized Pyrite in a Carbonate Medium. *Appl. Surf. Sci.* **2000**, *165*, 288−302.
(26) Guo, S.-P.; Li, J.-C.; Xiao, J.-R.; Xue, H.-G. Fe_3S_4 Nanoparticles Wrapped in an rGO Matrix for Promising Energy Storage: Outstanding Cyclic and Rate Performance. *ACS Appl. Mater. Interfaces* **2017**, *9*, 37694−37701.
(27) Morales-Gallardo, M. V.; Ayala, A. M.; Pal, M.; Cortes Jacome, M. A.; Toledo Antonio, J. A.; Mathews, N. R. Synthesis of Pyrite FeS_2 Nanorods by Simple Hydrothermal Method and its Photocatalytic Activity. *Chem. Phys. Lett.* **2016**, *660*, 93−98.
(28) Wang, Y.; Qian, X.; Zhou, W.; Liao, H.; Cheng, S. Hierarchical Nanostructured FeS_2 Hollow Microspheres for Lithium-ion Batteries. *RSC Adv.* **2014**, *4*, 36597−36602.
(29) Zhu, Y.; Fan, X.; Suo, L.; Luo, C.; Gao, T.; Wang, C. Electrospun FeS_2@carbon Fiber Electrode as a High Energy Density Cathode for Rechargeable Lithium Batteries. *ACS Nano* **2016**, *10*, 1529−1538.
(30) Son, S.-B.; Yersak, T. A.; Piper, D. M.; Kim, S. C.; Kang, C. S.; Cho, J. S.; Suh, S.-S.; Kim, Y.-U.; Oh, K. H.; Lee, S.-H. A Stabilized PAN-FeS_2 Cathode with an EC/DEC Liquid Electrolyte. *Adv. Energy Mater.* **2014**, *4*, 1300961.
(31) Fong, R.; Dahn, J. R.; Jones, C. H. W. Electrochemistry of Pyrite-based Cathodes for Ambient Temperature Lithium Batteries. *J. Electrochem. Soc.* **1989**, *136*, 3206−3210.
(32) Yersak, T. A.; Macpherson, H. A.; Kim, S. C.; Le, V.-D.; Kang, C. S.; Son, S.-B.; Kim, Y.-H.; Trevey, J. E.; Oh, K. H.; Stoldt, C.; Lee, S.-H. Solid State Enabled Reversible Four Electron Storage. *Adv. Energy Mater.* **2013**, *3*, 120−127.
(33) Xu, X.; Liu, J.; Liu, Z.; Shen, J.; Hu, R.; Liu, J.; Ouyang, L.; Zhang, L.; Zhu, M. Robust Pitaya-Structured Pyrite as High Energy Density Cathode for High-Rate Lithium Batteries. *ACS Nano* **2017**, *11*, 9033−9040.
(34) Tong, W.; Huang, Y.; Jia, W.; Wang, X.; Guo, Y.; Sun, Z.; Jia, D.; Zong, J. Leaf-like Interconnected Network Structure of MWCNT/Co_9S_8/S for Lithium-Sulfur Batteries. *J. Alloys Compd.* **2018**, *731*, 964−970.
(35) Xu, G.; Ding, B.; Nie, P.; Shen, L.; Dou, H.; Zhang, X. Hierarchically Porous Carbon Encapsulating Sulfur as a Superior Cathode Material for High Performance Lithium-Sulfur Batteries. *ACS Appl. Mater. Interfaces* **2014**, *6*, 194−199.
(36) Bugga, R. V.; Jones, S. C.; Pasalic, J.; Seu, C. S.; Jones, J.-P.; Torres, L. Metal Sulfide-Blended Sulfur Cathodes in High Energy Lithium-Sulfur Cells. *J. Electrochem. Soc.* **2016**, *164*, A265−A276.
(37) Ding, B.; Yuan, C.; Shen, L.; Xu, G.; Nie, P.; Zhang, X. Encapsulating Sulfur into Hierarchically Ordered Porous Carbon as a High-Performance Cathode for Lithium-Sulfur Batteries. *Chem. - Eur. J.* **2013**, *19*, 1013−1019.
(38) Ji, X.; Nazar, L. F. Advances in Li-S Batteries. *J. Mater. Chem.* **2010**, *20*, 9821−9826.
(39) Xu, X.; Meng, Z.; Zhu, X.; Zhang, S.; Han, W.-Q. Biomass Carbon Composited FeS_2 as Cathode Materials for High-Rate Rechargeable Lithium-ion Battery. *J. Power Sources* **2018**, *380*, 12−17.
(40) Whiteley, J. M.; Hafner, S.; Han, S. S.; Kim, S. C.; Oh, K. H.; Lee, S.-H. FeS_2-Imbedded Mixed Conducting Matrix as a Solid Battery Cathode. *Adv. Energy Mater.* **2016**, *6*, 1600495.
(41) Zhang, C.; Lin, Y.; Liu, J. Sulfur Double Locked by a Macro-Structural Cathode and a Solid Polymer Electrolyte for Lithium-Sulfur Batteries. *J. Mater. Chem. A* **2015**, *3*, 10760−10766.
(42) Zhang, Q.; Huang, N.; Huang, Z.; Cai, L.; Wu, J.; Yao, X. CNTs@S Composite as Cathode for All-Solid-State Lithium-Sulfur Batteries with Ultralong Cycle Life. *J. Energy Chem.* **2020**, *40*, 151−155.
(43) Zhou, C.; Bag, S.; He, T.; Lv, B.; Thangadurai, V. A 20 °C Operating High Capacity Solid-State Li-S Battery with an Engineered Carbon Support Cathode Structure. *Appl. Mater. Today* **2020**, *19*, 100585.
(44) Nagao, M.; Hayashi, A.; Tatsumisago, M. Sulfur-Carbon Composite Electrode for All-Solid-State Li/S Battery with Li_2S-P_2S_5 Solid Electrolyte. *Electrochim. Acta* **2011**, *56*, 6055−6059.
(45) Zhu, P.; Yan, C.; Zhu, J.; Zang, J.; Li, Y.; Jia, H.; Dong, X.; Du, Z.; Zhang, C.; Wu, N.; Dirican, M.; Zhang, X. Flexible Electrolyte-Cathode Bilayer Framework with Stabilized Interface for Room-Temperature All-Solid-State Lithium-Sulfur Batteries. *Energy Storage Mater.* **2019**, *17*, 220−225.
(46) Hou, L.-P.; Yuan, H.; Zhao, C.-Z.; Xu, L.; Zhu, G.-L.; Nan, H.-X.; Cheng, X.-B.; Liu, Q.-B.; He, C.-X.; Huang, J.-Q.; Zhang, Q. Improved Interfacial Electronic Contacts Powering High Sulfur Utilization in All-Solid-State Lithium-Sulfur Batteries. *Energy Storage Mater.* **2020**, *25*, 436−442.
(47) Yi, J.; Chen, L.; Liu, Y.; Geng, H.; Fan, L.-Z. High Capacity and Superior Cyclic Performances of All-Solid-State Lithium-Sulfur Batteries Enabled by a High-Conductivity $Li_{10}SnP_2S_{12}$ Solid Electrolyte. *ACS Appl. Mater. Interfaces* **2019**, *11*, 36774−36781.
(48) Zhang, C.; Lin, Y.; Zhu, Y.; Zhang, Z.; Liu, J. Improved Lithium-ion and Electrically Conductive Sulfur Cathode for All-Solid-State Lithium-Sulfur Batteries. *RSC Adv.* **2017**, *7*, 19231−19236.
(49) Sakuda, A.; Sato, Y.; Hayashi, A.; Tatsumisago, M. Sulfur-Based Composite Electrode with Interconnected Mesoporous Carbon for All-Solid-State Lithium-Sulfur Batteries. *Energy Technol.* **2019**, *7*, 1900077.

https://dx.doi.org/10.1021/acsami.0c01607
ACS Appl. Mater. Interfaces XXXX, XXX, XXX−XXX